PAPER • OPEN ACCESS

Gyrokinetic profile prediction and validation of a negative triangularity plasma in ASDEX Upgrade

OPEN ACCESS
IOP Publishing | International Atomic Energy Agency
Nuclear Fusion
Nucl. Fusion **65** (2025) 086042 (14pp)
https://doi.org/10.1088/1741-4326/adef68

Gyrokinetic profile prediction and validation of a negative triangularity plasma in ASDEX Upgrade

R. Bielajew[1,6,*], B. Vanovac[1], N.T. Howard[1], P. Rodriguez-Fernandez[1], L. Aucone[2], G.D. Conway[3], T. Happel[3], C. Holland[4], P. Mantica[5], J. Schellpfeffer[1], C. Yoo[1], A.E. White[1], the EUROfusion WPTE Team[a] and the ASDEX Upgrade Team[b]

[1] Plasma Science and Fusion Center, Massachusetts Institute of Technology, Cambridge, MA, United States of America
[2] Department of Physics 'G. Occhialini', University of Milano-Bicocca, Milano, Italy
[3] Max Planck Institute for Plasma Physics, Garching, Germany
[4] University of California, San Diago, CA, United States of America
[5] Istituto per la Scienza e Tecnologia dei Plasmi, CNR, Milano, Italy

E-mail: bielajew@mit.edu and rbielajew@rutherfordev.com

Received 28 March 2025, revised 5 July 2025
Accepted for publication 14 July 2025
Published 28 July 2025

Abstract

In this work, gyrokinetic simulations are performed with the CGYRO code (Candy *et al* 2016 *J. Comput. Phys.* **324** 73–93) for a negative triangularity H-mode plasma in ASDEX Upgrade, and compared with experimental measurements. The PORTALS framework (Rodriguez-Fernandez *et al* 2024 *Nucl. Fusion* **64** 076034) is used to accelerate the prediction of kinetic profiles for this plasma, using surrogate modeling and Bayesian optimization. Ion heat flux, electron heat flux, and electron particle flux are simultaneously matched across the simulated radial regime of the plasma (normalized radius $r/a = 0.35 - 0.90$), and the resulting ion temperature, electron temperature, and electron density profiles match well with the experimental profile data within this radial range. A synthetic Correlation Electron Cyclotron Emission diagnostic is applied to find well-matched electron temperature fluctuation properties between simulation and experiment. The flux-matched profiles provide a basis for investigation of the turbulence nature across the plasma radius, revealing the dominance of Trapped Electron Mode turbulence at $r/a = 0.35$, the dominance of Ion Temperature Gradient turbulence at $r/a = 0.55$, 0.75, and 0.83, and an instability boundary at $r/a = 0.90$.

[6] Present address: Rutherford Energy Ventures.
[a] See Joffrin *et al* 2024 (https://doi.org/10.1088/1741-4326/ad2be4) for the EUROfusion WPTE Team.
[b] See Zohm *et al* 2024 (https://doi.org/10.1088/1741-4326/ad249d) for the ASDEX Upgrade Team.
[*] Author to whom any correspondence should be addressed.

Keywords: gyrokinetic simulation, turbulence, transport, synthetic diagnostics, negative triangularity

(Some figures may appear in colour only in the online journal)

1. Introduction

The prediction of future tokamak operation depends on accurately modeling the heat and particle transport processes of the confined plasma. Turbulence is known to drive the majority of transport in the confined plasma region [1]. This turbulent transport may be represented, and simulated, at high fidelity with the gyrokinetic model. Recent advances in integrated modeling [2] have enabled the use of local, δf gyrokinetic codes to predict the plasma transport and kinetic profiles simultaneously across multiple channels. These full profile simulations allow performance predictions of future burning plasma experiments and pilot power plants with increased confidence [3–5].

To ensure confidence in the predictive modeling for future reactors, validation of transport models is performed on current machines [6]. The PORTALS-CGYRO integrated modeling framework [2] enables the use of gyrokinetic codes to predict kinetic profiles that match fluxes across multiple channels between the transport (turbulent and neoclassical) and target (from sources and sinks, such as heating, exchange power and radiation). Simulations performed with these flux-matched profiles provide a basis for comparing simulated turbulence with experimental turbulence measurements. Comparison between measured and simulated transport fluxes is routine, but comparison across more fundamental turbulence quantities, such as the fluctuation spectra and amplitude, is less frequently performed. Recent validation work assisted by PORTALS has demonstrated the value of these flux-matched turbulence comparisons [5].

Recent experiments at The ASDEX Upgrade Tokamak (AUG) targeted negative triangularity (NT) shaping [7, 8]. On this machine, shaping is modest with the average triangularity δ_{av} not extending beyond -0.2. At this modest NT shaping, ELMs can occur, although the properties of these NT ELMs are not explained by ideal peeling-ballooning stability analysis alone [8]. AUG NT plasmas have also been the subject of recent modeling work, including a prediction of kinetic profiles through the ASTRA-TGLF framework [9]. Gyrokinetic modeling has been used to study NT plasmas with L-mode like edges at the TCV [10–13] and DIII-D [14] tokamaks. The gyrokinetic modeling of AUG NT plasmas has so far been limited to linear simulations [7]. The results to be presented here are the first nonlinear gyrokinetic simulations for NT at AUG, and the first ever gyrokinetic profile prediction in NT.

In this paper, we present a nonlinear gyrokinetic study of an AUG NT plasma. The experiment used as a basis is described in section 2, including the experimental turbulence measurements. Five radial locations (defined in terms of minor radius, r, normalized to the radius of the last closed flux surface, a) are simulated between $r/a = 0.35$ and 0.90 using the CGYRO code [15]. The PORTALS framework is used to accelerate the convergence of the turbulent and neoclassical transport fluxes to the target flux values and determine the flux-matched ion temperature (T_i), electron temperature (T_e), and electron density (n_e) profiles. The modeling methodology is described in section 3. A synthetic Correlation Electron Cyclotron Emission (CECE) diagnostic is applied to the flux-matched profiles to compare simulated turbulence with experimental measurements, as described in section 4. An investigation of the nature of turbulence at the different simulated radii is presented in section 5. A summary and discussion is given in section 6.

2. NT experiment and turbulence measurements

The discharge studied in this work was performed in AUG. Selected time traces and the equilibrium of this discharge are shown in figure 1. This experiment was performed with magnetic field on axis $B_T = 2.5$ T, plasma current $I_p = 0.8$ MA, safety factor at the flux surface that encloses 95% of the poloidal flux $q_{95} = 4.7$, and line averaged density $n_e = 5.47 \times 10^{19}$ m^{-3}. The safety factor on axis q_0 was below 1, resulting in sawteeth. The plasma was heated with 3.0 MW of Electron Cyclotron Resonance Heating (ECRH) and 4.1 MW of Neutral Beam Injection (NBI). NT shaping was achieved on average with average triangularity $\delta_{\text{average}} = -0.14$, although the upper triangularity $\delta_{\text{upper}} = -0.33$ and the lower triangularity $\delta_{\text{lower}} = 0.05$. The steady-state period chosen for modeling is 3.1–3.5 s, shown as the shaded region in the time histories of figure 1. The plasma is ELMing during this phase. Interpretive TRANSP [16] was run to determine that Q_i is higher than Q_e over the majority of the plasma radius during the steady-state H-mode phase of this plasma. Measurements of radial profiles were performed with Thomson scattering [17] and ECE [18] for the T_e profile, Thomson scattering for the n_e profile, and Charge Exchange Recombination Spectroscopy (CXRS) [19, 20] for the T_i and v_{tor} profiles.

2.1. T_e fluctuation measurements

Turbulent T_e fluctuations were measured using the CECE diagnostic [21, 22]. At the time of this experiment, the CECE system was comprised of 32 radial channels, capable of measuring T_e fluctuations with high radial resolution over a range of $\rho_{\text{tor}} \approx 0.7 - 1.0$. Within this radial range, T_e fluctuation spectra are produced from correlating radially neighboring

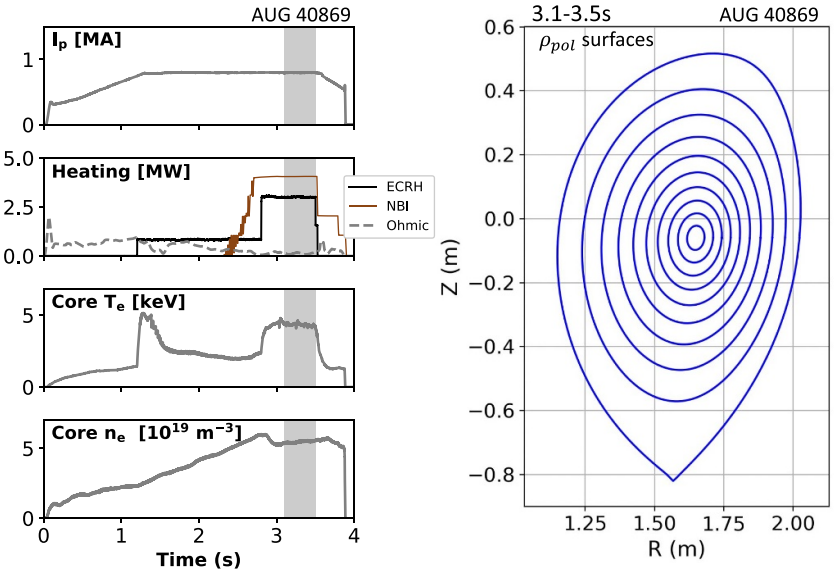

Figure 1. Overview of the negative triangularity discharge #40869. Time traces include current, heating (ECRH, NBI, and Ohmic), core T_e, and core n_e. The equilibrium reconstruction is shown with contours of ρ_{pol}.

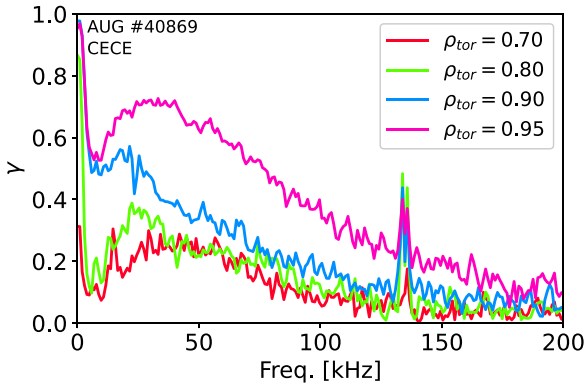

Figure 2. Coherence (γ) spectra of T_e fluctuations at selected radial locations in the outer core and edge, measured with CECE. The spike at 140 kHz is due to electronic noise.

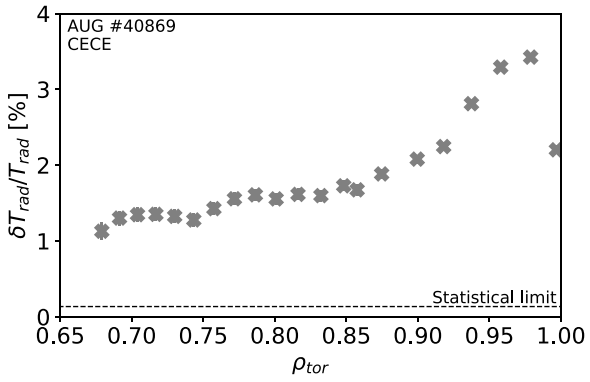

Figure 3. $\delta T_{\mathrm{rad}}/T_{\mathrm{rad}}$ fluctuation amplitude over radius, measured with CECE.

channels. Figure 2 shows coherence (γ) spectra from selected radial locations in the plasma outer core, pedestal top, and pedestal region. Inside the pedestal ($\rho_{\mathrm{tor}} \leqslant 0.90$), turbulent features are seen in the coherence spectra in the range of 5–100 kHz. In the pedestal region ($\rho_{\mathrm{tor}} > 0.90$) the turbulent feature has a high value of coherence and a frequency breadth to 200 kHz. Figure 3 shows a radial profile of the $\delta T_{\mathrm{rad}}/T_{\mathrm{rad}}$ fluctuation amplitude. The fluctuation amplitude is seen to increase from near 1% in the outer core to above 3% in the pedestal region. For these fluctuation amplitudes, the radiated temperature T_{rad} is used instead of the electron temperature T_e because near the separatrix ($\rho_{\mathrm{tor}} \geqslant 0.99$) the plasma is optically thin, so $\delta T_{\mathrm{rad}}/T_{\mathrm{rad}}$ may have a contribution from n_e fluctuations in addition to T_e fluctuations [23]. When the plasma is optically thick ($\rho_{\mathrm{tor}} < 0.99$), $\delta T_{\mathrm{rad}}/T_{\mathrm{rad}} = \delta T_e/T_e$.

3. Modeling methodology for flux matched simulations

Gyrokinetic simulations are run with the CGYRO code [15], and the PORTALS framework [2] is used to accelerate the convergence of computed heat and particle transport fluxes to target values. CGYRO is a local, Eulerian, spectral gyrokinetic code, with a wide user base in tokamak turbulent transport modeling. It is designed for collisional, electromagnetic, multiscale simulations, and is optimized for performance on modern computing architectures, such as high-performance GPU-accelerated systems.

3.1. Gyrokinetic simulation setup

Nonlinear gyrokinetic simulations were run at 5 radial locations ($r/a = 0.35, 0.55, 0.75, 0.83, 0.90$). These radial

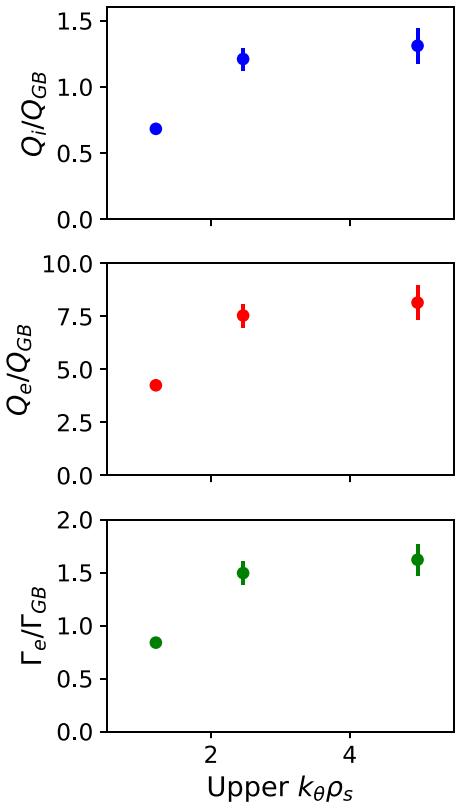

Figure 4. Nonlinear Q_i, Q_e, and Γ_e normalized to gyroBohm units, for simulations with varying $k_\theta\rho_s$ ranges. The upper limit of $k_\theta\rho_s$ is indicated on the x-axis.

locations were selected based on the study presented in [2] showing that this choice of radii is optimal for inductive plasmas with on-axis heating. In this experiment, the largest sawteeth have an effect on profiles up to normalized radius $r/a = 0.50$. While the reconstructed profiles at $r/a = 0.35$ are affected by sawteeth, the points $r/a = 0.55$ and outward are unaffected. Wavenumbers in the range $k_\theta\rho_s = 0.1$ to 2.5 were included at all locations, where k_θ is the poloidal wavenumber and ρ_s is the ion gyroradius evaluated at the ion sound speed. Ion-scale simulations are expected to be sufficient for capturing turbulent fluxes because an interpretive TRANSP calculation indicates that Q_i is dominant over Q_e in the simulated region, and it will be shown in section 5 that the dominant mode linear growth rates normalized to wave numbers are higher at the ion scale than the electron scale. The chosen wavenumber range for the nonlinear simulations is slightly larger than that for a typical ion scale simulation, which often include wavenumbers only as high as $k_\theta\rho_s = 1.2$. Scans of the wavenumber range indicate that the increased range is needed to capture an accurate representation of the turbulent fluxes, especially at the innermost radial location. Figure 4 shows a scan of the ion and electron heat fluxes and the electron particle flux from a range of simulations in which the maximum wavenumber is varied from $k_\theta\rho_s = 1.2$ to 5.0. The fluxes nearly double between $k_\theta\rho_s = 1.2$ and 2.5 as a maximum wavenumber, but do not change significantly with a further increase in wavenumber range. By including a wider $k_\theta\rho_s$ spectrum, TEM turbulence is better captured. This increased wavenumber range increases the computational cost of these simulations.

The radial domain sizes $L_x \times L_y$ were approximately $120 \times 90\rho_s$, and scans of the domain size confirmed that there was less than $<1\%$ change in fluxes compared to a domain size of $120 \times 120\rho_s$. Approximately 512 radial modes were used for each simulation, although this varied between radial locations. For each simulation, 24 poloidal θ gridpoints, 24 pitch angle ξ gridpoints, and 8 energy gridpoints were used. The simulations included electrostatic ($\delta\phi$) and electromagnetic ($\delta A_\parallel$) perturbations, although $\delta B_\parallel$ perturbations were not included. The inclusion of $\delta B_\parallel$ perturbations was found not to change the nonlinear turbulent fluxes beyond a standard deviation. The geometry was included with a Miller extended harmonic (MHX) parametrization [24], which can capture up-down asymmetry. The Sugama collision operator is used and rotation effects such as $E \times B$ shearing are retained. Three gyrokinetic species were evolved: ions, electrons, and a lumped impurity with charge $Z = 5.7$ and mass $A = 11.3$. The lumped impurity species is meant to represent an average impurity that includes contributions from W and B, with fractions determined from experimental measurements of Z_{eff} and tungsten concentration.

3.2. *Profile predictions through the PORTALS framework*

The PORTALS framework uses surrogate modeling to accelerate profile predictions using high-fidelity gyrokinetic simulations to calculate turbulent transport fluxes. The framework is described in detail in [2]. To summarize, to solve for kinetic n_e, T_e, and T_i profiles, the inverse gradient scale lengths are treated as the free parameter and a coupled system of energy and particle conservation equations are solved. Profiles are determined by minimizing the difference between transport fluxes (from turbulent and neoclassical transport) and target fluxes (from particle and energy sources and sinks, such as heating and energy exchange). Both the target and transport fluxes depend on the details of the kinetic profiles.

For the target fluxes, auxiliary heating profiles calculated by TRANSP were held constant, and radiation and collisional exchange were calculated self-consistently at each step. For the transport fluxes, CGYRO was used to evaluate the turbulent contributions to Q_i, Q_e, and Γ_e and the neoclassical code NEO [25] was used to calculate the neoclassical contributions. PORTALS uses an initial set of $\sim$5 simulations to fit a Gaussian Process model to represent the turbulent transport fluxes versus local plasma parameters and the residual to minimize. After this initial training phase, the surrogate model is used to predict the set of input parameters where flux matched conditions will be found. The next set of gyrokinetic simulations is run for these predicted inputs. If the transport fluxes match the simulated target fluxes within a chosen criterion, such as two times the standard deviation (2σ), the

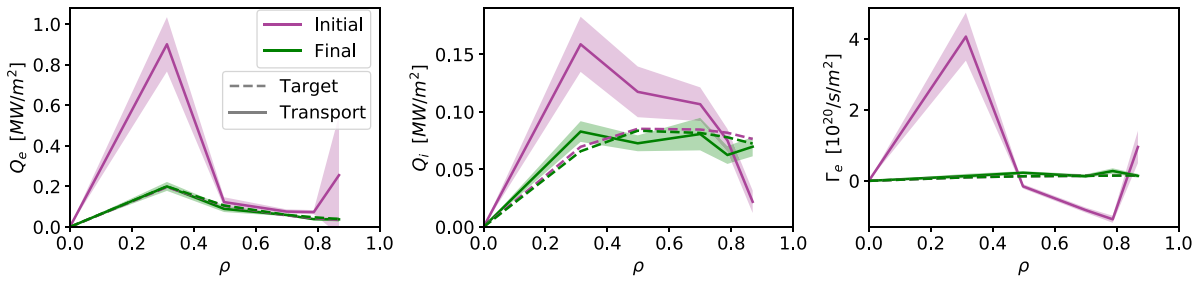

Figure 5. A comparison of target fluxes (dashed) and transport fluxes (solid), with 2σ uncertainties on the transport fluxes indicated with shading. Fluxes from the initial profiles are in purple and the final profiles are in green. The radial coordinate ρ is the square root of the normalized toroidal flux.

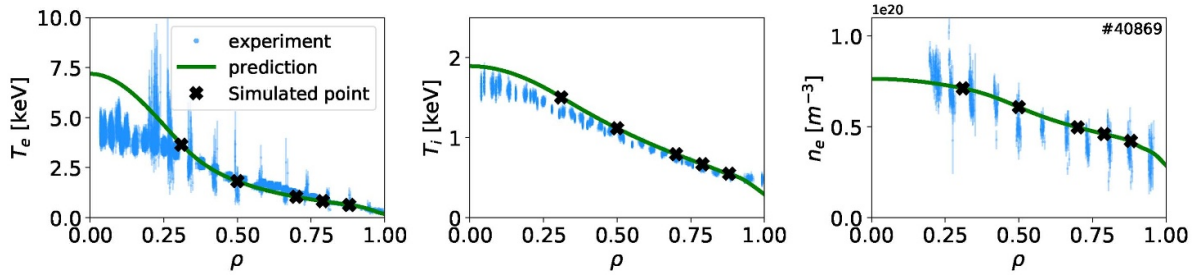

Figure 6. The final kinetic profiles calculated from PORTALS-CGYRO (green) are shown with the experimental profile measurements (blue). The simulated points are indicated with black Xs. The radial coordinate ρ is the square root of the normalized toroidal flux.

kinetic profiles are considered converged. If the transport and target fluxes do not match, then the additional simulation is added to the surrogate model and a new point is predicted for flux matching conditions.

For the simulations presented here, 17 evaluations of CGYRO were performed at each of the 5 radii in order to arrive at flux matched profile predictions, for a total of 85 simulations. The nonlinear simulations were run based on a saturated startup simulation from an initial set of profiles, and typically run for an additional $\sim$350 a/c_s (where the time unit a/c_s is the minor radius over the sound speed), although the exact run lengths varied between simulations. A comparison of the initial and converged target and transport fluxes is shown in figure 5. The initial transport fluxes are seen to be far from target values, but good agreement is found after the 17 CGYRO evaluations. At some points, the transport fluxes are more than 2σ from the target values (the largest deviations being 4σ in the ion heat flux channel at the $r/a = 0.35$ and 0.83 locations), but continuing this process results in vanishingly small predicted changes to the input gradients and the match was considered close enough not to justify further simulations.

4. Comparison between simulations and experiment

4.1. Profile comparison

The flux-matched profiles agree well with experimental measurements. Figure 6 shows the PORTALS-CGYRO prediction alongside measurements of T_e, T_i, and n_e. The points simulated with CGYRO are shown with black X's. The profiles in the region outside the outermost point ($r/a = 0.90$) are held fixed. The profiles are constructed by smoothly interpolating the gradient scale lengths between the simulated points, then integrating from the outermost point inwards. Inside the innermost point ($r/a = 0.35$) the profiles are constructed by linearly interpolating the gradient scale lengths to 0 at $r/a = 0$. Within the region simulated ($r/a = 0.35 - 0.90$), the predicted T_e and n_e profiles fall well within the scatter of the experimental data, and the T_i predicted profile is only above the scatter of the data at the innermost point. In the deep core region that is not simulated ($r/a < 0.35$), the predicted T_e profile is higher than the experimental measurements. However, we emphasize that this region is not represented with gyrokinetic simulations in this study, and sawteeth are not included when constructing the deep core profile although they are present in the experiment. In the experiment, the sawtooth time period is less than the energy confinement time, so the core profile relaxation due to sawteeth likely contributes to the disagreement between experiment and prediction in this region.

4.2. T_e fluctuation comparisons

Profiles flux matched in Q_e, Q_i, and Γ_e provide a valuable basis for comparing simulated turbulence with experimental measurements. The spectra, fluctuation amplitude, and correlation length are fundamental characteristics of turbulence that provide stringent tests of the gyrokinetic model when simulations are compared with experiment. These turbulence properties occupy a more fundamental level of the 'primacy

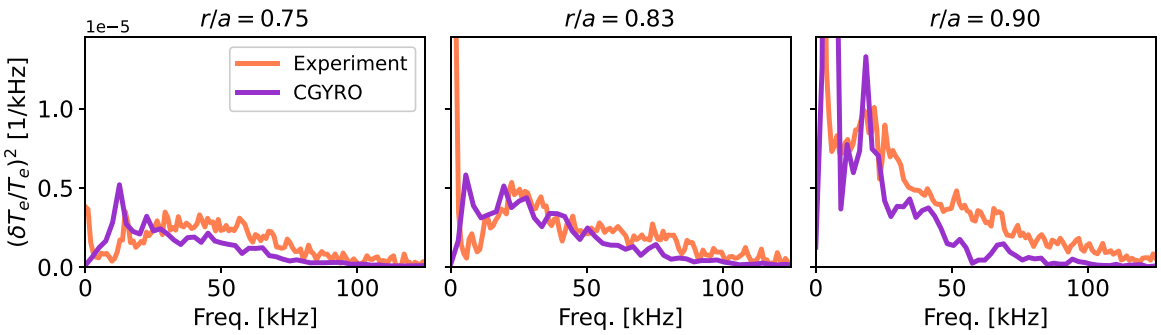

Figure 7. Comparison of the crosspower G_{xy} between simulation (purple) and experiment (orange) at three radial locations.

hierarchy' [26], compared to fluxes which must be calculated from a number of measurements all with their own uncertainties. The T_e fluctuation spectra, $\delta T_e/T_e$ fluctuation amplitude, and T_e fluctuation correlation length are compared between simulation and experiment by applying a synthetic CECE diagnostic to the CGYRO simulations. The plasma is optically thick at all locations chosen for simulation, so $\delta T_{\mathrm{rad}}/T_{\mathrm{rad}} = \delta T_e/T_e$ in experiment. The synthetic diagnostic is constructed by applying a point spread function to the CGYRO fluctuation outputs, mapped to R, Z space. The synthetic diagnostic was based on that in [27]. The point spread function representing the CECE diagnostic matches the geometry of the AUG CECE system, including the R and Z measurement locations, the measurement volumes, and the spacings between correlated channels. The simulations run for synthetic diagnostic purposes generally included a poloidal output grid of 24 points, and were run for steady state periods of at least 700 a/c_s in order to provide long time histories for statistical analysis.

Figure 7 shows the CECE cross-power spectra G_{xy} at the radial locations $r/a = 0.75$, 0.83, and 0.90. Experimental CECE measurements did not extend farther into the core for this experiment. The experimental CECE diagnostic is not a calibrated system. Therefore, the experimental frequency spectra are represented as in [28], by

$$\left(\frac{\delta T_e}{T_e}(f)\right)^2 = \frac{2}{B_{\mathrm{IF}}}\frac{|\gamma_c(f) - \gamma_{bg}|}{1 - |\gamma_c(f) - \gamma_{bg}|} \tag{1}$$

where γ_c and γ_{bg} are the complex and background coherence respectively and B_{IF} is the CECE IF filter bandwidth. For this discharge, γ_{bg} is the average coherence from 175 to 200 kHz, and represents instrument noise that is not present in the simulation. At $r/a = 0.90$, the simulation outputs only include a midplane poloidal location, due to the stability of the saturation of this simulation. As will be discussed in section 5, this point at $r/a = 0.90$ sits at an instability boundary and despite using the same input parameters, the simulation with only midplane outputs exhibited stable turbulence saturation while the simulation with multiple poloidal outputs did not. At $r/a = 0.83$, the synthetic CECE diagnostic is not applied to the full simulation time extent due to a slowly growing low wavenumber mode, which only becomes apparent after $a/c_s = 1000$. At all three locations, the shape of the spectra show good agreement between experiment and simulation, in terms of the spectral shape and amplitude.

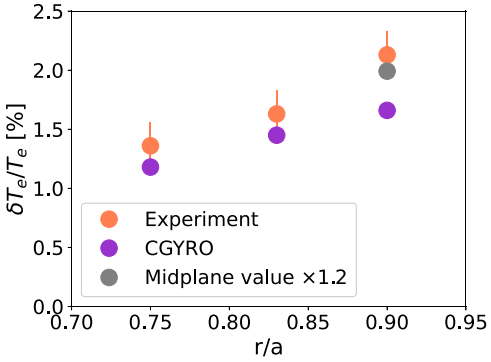

Figure 8. Comparison of the $\delta T_e/T_e$ fluctuation amplitude between experiment and simulation. 2σ error bars are shown on the experimental points. At $r/a = 0.90$, only fluctuations at the midplane are output, so the midplane value $\times 1.2$ is shown in gray to visualize an estimated $\delta T_e/T_e$ value at the diagnostic's (R, z) location.

The comparison of the $\delta T_e/T_e$ fluctuation amplitude between experiment and simulation for three radial locations is shown in figure 8. The fluctuation amplitude is calculated by integrating the cross-power spectrum over a frequency range of interest. For the experimental calculation, equation (1) is integrated. The frequency range of integration for both experiment and simulation was 5–175 kHz. The fluctuation amplitude matches within 2σ at $r/a = 0.75$ and 0.83. At $r/a = 0.90$, the experimental fluctuation amplitude is 22% smaller than the simulated one. We note that the simulation at $r/a = 0.90$ only included midplane fluctuations. When restricting the synthetic CECE diagnostic at $r/a = 0.75$ and 0.83 to only include midplane fluctuations, the simulated fluctuation amplitudes are decreased by $\sim$20% at these locations as well. The slightly lower fluctuation levels and spectra observed in the synthetic diagnostic compared to experiment may be due to uncertainties in the modeled poloidal spot size, which can reduce sensitivity to smaller wavenumbers. Additionally, residual background noise in the experimental spectra, despite

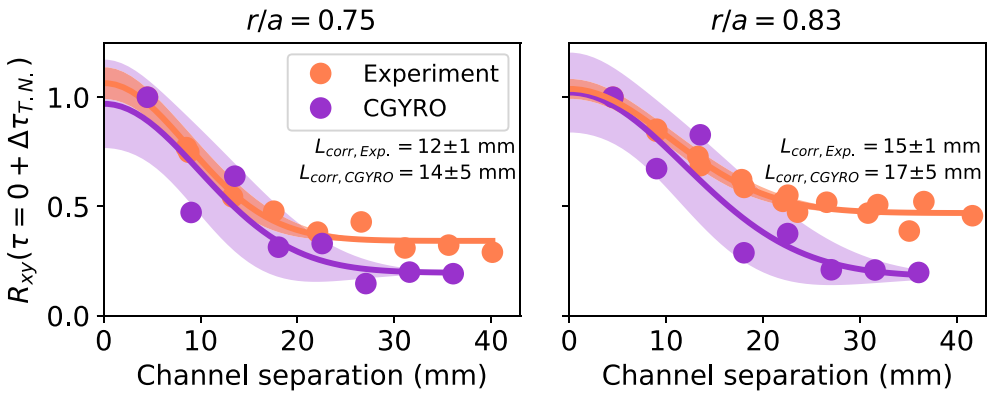

Figure 9. Comparison of the T_e fluctuation correlation length experiment and simulation at $r/a = 0.75$ and $r/a = 0.83$. The correlation coefficients at zero time delay plus a $\Delta\tau_{\text{T.N.}} = 1/B_{\text{vid}}$ modification to move outside the thermal noise peak are shown versus channel separation. The Gaussian fits to the correlation coefficients are also shown. 2σ errors on the fits are indicated with the shaded regions.

background subtraction applied (equation (1)), may contribute to a systematic offset in the measured amplitude.

The correlation length, L_{corr}, is typically determined by computing the cross-correlation coefficient at zero time delay of sequential CECE channels, $R_{xy}(\tau = 0)$. L_{corr} is defined here as the $1/e^2$ width of a Gaussian fit to the correlation coefficients versus radial separation between the channels. To avoid contributions from thermal noise in the experimental case, a slightly modified time delay $\tau = 0 + \Delta\tau_{\text{T.N.}}$ is used, where $\Delta\tau_{\text{T.N.}} = 1/B_{\text{vid}}$ is the width of the thermal noise peak. B_{vid} is the video bandwidth of the experimental system.

Figure 9 shows both the correlation coefficients and the Gaussian fit to these at $r/a = 0.75$ and 0.83. The correlation length is not fit to the point at $r/a = 0.90$ due to the limited number of CECE channels in the simulation domain at this radial location. The correlation coefficients are normalized to the same maximum value for ease of plotting. The correlation coefficients versus radial separation can be fit to a Gaussian in both experiment and simulation. The experimental correlation coefficients have a higher background value at a large distance >20 mm compared to simulation. The time-delay correlation method R_{xy} correlates the entire spectrum up to the Nyqist frequency, so this background may be a result of correlated noise not successfully removed by avoiding the thermal noise peak with a $\Delta\tau_{\text{T.N.}}$ time delay modification. Despite this higher experimental background, the $1/e^2$ width of the Gaussian fits to the experimental and simulation correlation coefficients are within 2σ at both radial locations. Overall, in terms of spectral characteristics, $\delta T_e/T_e$ fluctuation amplitude, and L_{corr}, the simulation and experiment are well matched.

There is good agreement between the CGYRO simulations and experimental measurements in terms of kinetic profile predictions, and T_e fluctuation characteristics. This detailed validation shows that the core of NT plasmas of this type can be accurately represented with the gyrokinetic model.

5. Turbulence nature across the plasma radius

An investigation of the nature of the simulated turbulence was conducted by performing additional simulations for the

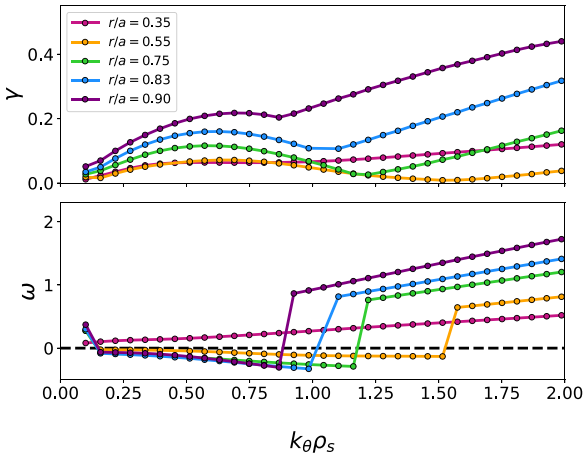

Figure 10. Linear stability analysis of the five simulated radial locations, performed with the flux-matched profiles. The dominant mode growth rate (γ) and real frequency (ω) are shown, both in units of c_s/a—the ion sound speed normalized to the minor radius. Ion/electron modes are in the $-\omega/+\omega$ direction.

flux-matched profiles. To understand the linear properties of the dominant instabilities in this plasma, linear CGYRO simulations were performed. The dominant mode linear growth rates (γ) and real frequencies (ω) over a range of $k_\theta\rho_s$ are shown in figure 10. At $r/a = 0.55 - 0.90$, the Ion Temperature Gradient (ITG) instability is dominant for the low $k_\theta\rho_s$ portion of the spectrum, although a micro-tearing mode (MTM) is present at $k_\theta\rho_s = 0.1$.

The MTM is identified through the structure of the mode with respect to the ballooning angle θ. Figure 11 shows the tearing structure of the dominant mode at $k_\theta\rho_s = 0.1$, with ϕ with odd parity and $A_\parallel$ with even parity (both real and imaginary components). A comparison of the sensitivity of the growth rate to β and collision frequency ν_{ee} at $k_\theta\rho_s = 0.1$ and $k_\theta\rho_s = 0.5$ at the radial location $r/a = 0.75$ is shown in figure 12. Here, β refers to the electron β_e and is calculated with respect to B_{unit}. The β and ν_{ee} are varied $\pm 50\%$ relative to the converged point values. At $k_\theta\rho_s = 0.1$, where the MTM is the dominant mode, the growth rate increases with

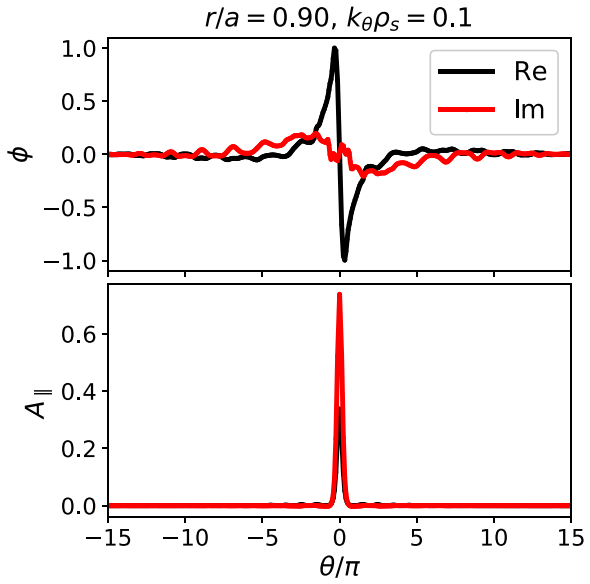

Figure 11. The real and imaginary components of the linear dominant mode ϕ and $A_\parallel$ with respect to the ballooning angle θ at $k_\theta\rho_s = 0.1$ at $r/a = 0.90$, for the flux-matched profiles.

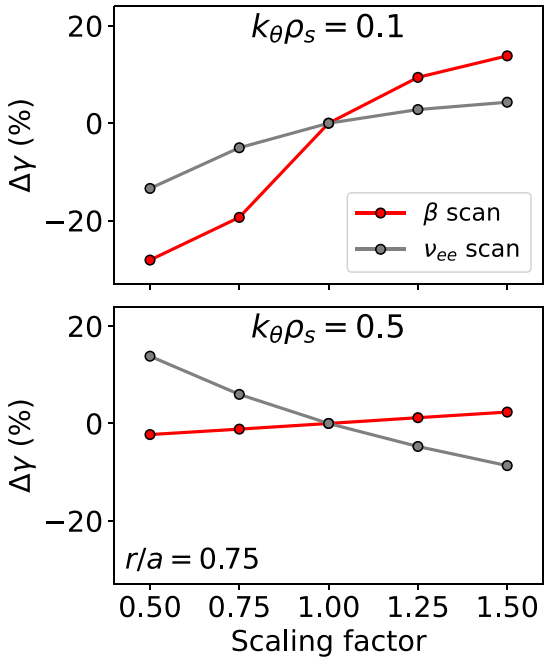

Figure 12. The change in γ as the β_e and ν_{ee} input parameters are varied by $\pm 50\%$ around the converged point at wavenumbers $k_\theta\rho_s = 0.1$ and 0.5 at the radial location $r/a = 0.75$. The converged point values are $\beta_e = 1.39 \times 10^{-3}$ and $\nu_{ee} = 1.84 \times 10^{-1}$ $[c_s/a]$.

increasing β and ν_{ee}. At $k_\theta\rho_s = 0.5$, where ITG is dominant, the growth rate is largely insensitive to β and decreases with ν_{ee}. Linear scans of a/L_{T_e}, a/L_{T_i}, and a/L_n at $k_\theta\rho_s = 0.1$ also indicate that the MTM growth rate increases with increasing a/L_{T_e} and decreases with increasing a/L_n. The MTM growth rate is insensitive to a/L_n.

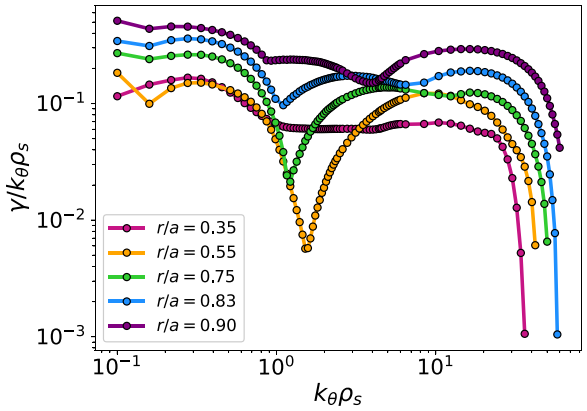

Figure 13. Growth rate normalized to $k_\theta\rho_s$ shown over both the ion scale $k_\theta\rho_s < 1.0$ and electron scale $k_\theta\rho_s > 1.0$ ranges, for the flux-matched profiles.

In contrast to the ITG present at the other locations, at $r/a = 0.35$, TEM is dominant for the entire ion-scale portion of the $k_\theta\rho_s$ spectrum, as indicated by the electron directed real frequency. Linear scans of the case at $r/a = 0.35$ show that at low wavenumbers, the linear growth rate is most sensitive to a/L_{T_e}, indicating an electron temperature gradient driven TEM.

Linear stability analysis was also run at the electron scale ($k_\theta\rho_s > 1.0$), to understand the potential importance of high-k turbulence in these simulations. The linear growth rate normalized to wavenumber, $\gamma/k_\theta\rho_s$, is shown in figure 13. At all radial locations the peak of $\gamma/k_\theta\rho_s$ at the ion scale ($k_\theta\rho_s < 1.0$) exceeds the peak value of $\gamma/k_\theta\rho_s$ at the electron scale. This indicates that cross-scale coupling effects are unlikely to be important in nonlinear simulations [29, 30].

The turbulence at $r/a = 0.90$ displays strong sensitivity to a/L_{T_e} both linearly and nonlinearly. Figure 14 shows scans of γ and ω for the point at $r/a = 0.90$. The gradient drive terms a/L_{T_e}, a/L_{T_i}, and a/L_n are all scanned $\pm 20\%$ around the flux-matched profiles 'base case'. The dominant mode linear stability is most strongly affected by a/L_{T_e}, although at low wavenumbers $k_\theta\rho_s < 1.0$, there was also an effect from a/L_{T_i} due to ITG destabilization. This can be seen in the a/L_{T_i} scan in figure 14, where linear growth rates increase with increasing a/L_{T_i} in the range of the spectrum where the real frequency is ion-directed. When a/L_{T_i} is reduced from the base case, the dominant mode transitions from ion-directed to electron-directed at a lower value of $k_\theta\rho_s$.

Scans of the nonlinear fluxes confirm the sensitivity of the turbulence to a/L_{T_e}, as shown in figure 15. These scans are performed by running additional nonlinear simulations with a/L_{T_e} adjusted $\pm 10\%$ around the converged base case. The turbulent Q_i, Q_e, and Γ_e fluxes all increase sharply upon a slight (5%) increase in a/L_{T_e}, indicating that the converged point sits at an instability boundary. The nature of the turbulence changes from primarily electrostatic when a/L_{T_e} is at the converged point or below, to strongly electromagnetic when a/L_{T_e} is above the converged point. Q_e is the most strongly

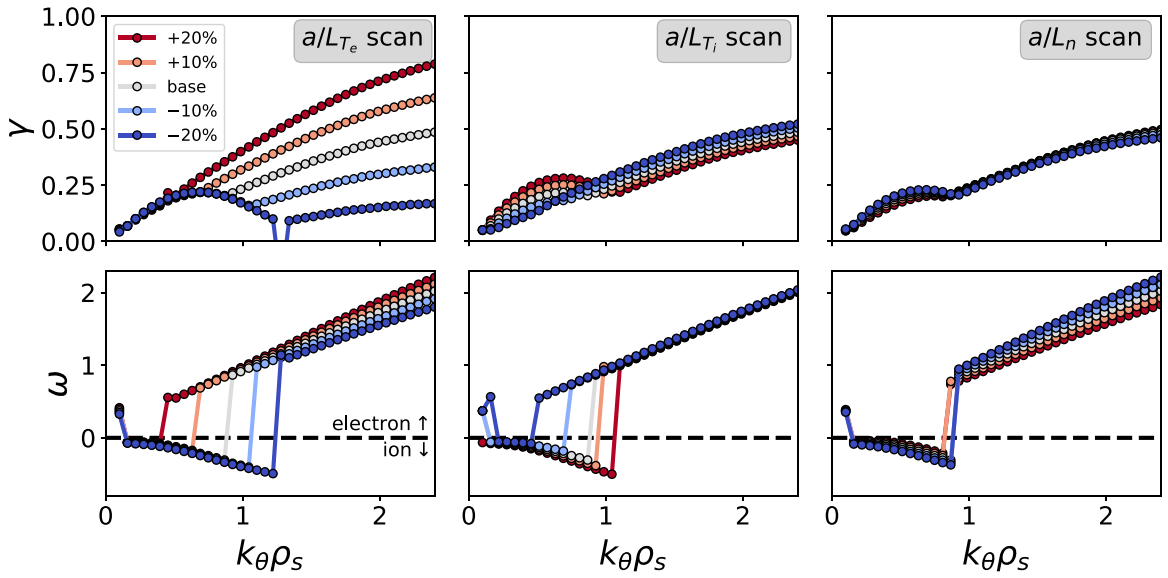

Figure 14. Linear growth rates and real frequencies (both in units of c_s/a) at $r/a = 0.90$ for scans of a/L_{T_e}, a/L_{T_i}, and a/L_n. Each gradient is scanned up to $\pm 20\%$ of the flux-matched case value.

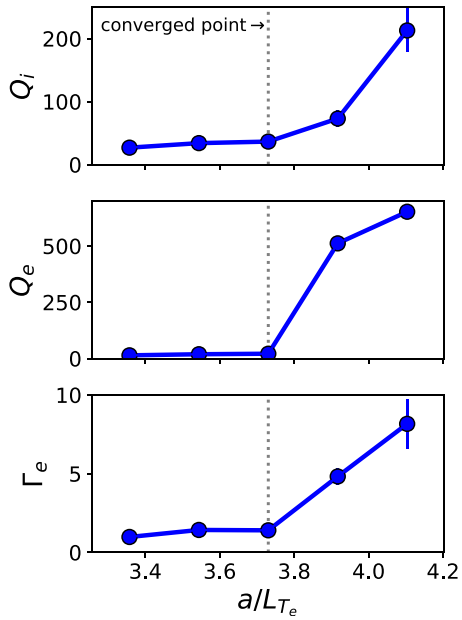

Figure 15. Q_i, Q_e, and Γ_e for a nonlinear scan around the flux-matched value of a/L_{T_e} at $r/a = 0.90$. All fluxes are shown in gyroBohm units.

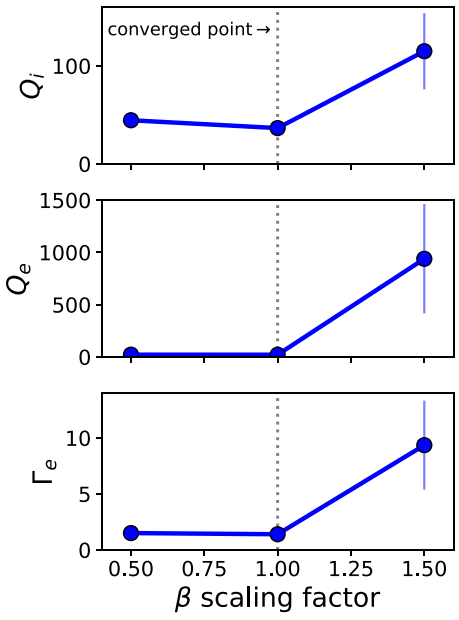

Figure 16. Q_i, Q_e, and Γ_e for a nonlinear scan around the flux-matched value of β_e at $r/a = 0.90$. All fluxes are shown in gyroBohm units.

affected flux. A similar instability threshold with respect to β was found with nonlinear scans varying β around the converged point, as shown in figure 16. When β is below the converged point value, there is little effect on the turbulent fluxes. When β is increased, Q_e, Q_i, and Γ_e all increase sharply, but the effect is strongest on Q_e.

The electromagnetic nature of this turbulence, sensitivity to β, sensitivity to a/L_{T_e} indicate that turbulence from MTMs may be important above the converged values of a/L_{T_e} and β. However, this trend is not entirely reproduced linearly, where MTMs are only present at lowest wavenumber and the linear growth rates do not exhibit an instability threshold relating to a/L_{T_e} or β, but rather the MTM linear growth rate increases monotonically with increasing a/L_{T_e} or β. We note that simulations with a/L_{T_e} or β above the value at the converged point do not reach a saturated steady-state due to the computational

cost of the strongly growing instabilities, so the fluxes shown in figures 15 and 16 should be taken as qualitative rather than quantitative values.

The sensitivity of turbulence to key parameters, such as gradient scale lengths, collisionality, and the ion to electron temperature ratio, can also be investigated using the surrogate model built in the process of PORTALS profile predictions. Rather than running additional expensive nonlinear gyrokinetic simulations, the surrogates relating the turbulent Q_e, Q_i, and Γ_e to inputs (a/L_{T_e}, a/L_{T_i}, a/L_n, ν_{ei}, and T_i/T_e) can be scanned around a given range of the converged solution's inputs. Scans using the surrogate models are shown in figure 17 for two representative locations ($r/a = 0.35$ and $r/a = 0.75$). At $r/a = 0.35$, increasing a/L_{T_e} is seen to increase Q_e and Γ_e while decreasing Q_i, while increasing a/L_{T_i} is seen to increase Q_i. This indicates a balance of TEM and ITG turbulence at this location. At $r/a = 0.75$, a/L_{T_i} most strongly drives both channels of heat flux, indicating strongly dominant ITG at this location. We note that these scans are approximate and should only be used for qualitative study because they are based on surrogates to complex dynamics of 5 inputs with just 17 CGYRO evaluations. These surrogates can be used as a tool for understanding the drivers of nonlinear fluxes at several locations, and when performing profile predictions for future reactors can be used as a means to cheaply investigate operating scenarios.

6. Summary and discussion

In this paper, gyrokinetic simulations are performed for a NT H-mode plasma in AUG. The PORTALS surrogate modeling technique is used to find convergence between turbulent and neoclassical transport fluxes and target fluxes (from sources and sinks), at a reduced computational cost compared to traditional transport solvers. Using this technique, Q_i, Q_e, and Γ_e were simultaneously matched across the simulated radial regime of the plasma ($r/a = 0.35 - 0.90$), and the resulting T_i, T_e, and n_e profiles match well with the experimental profile data within this radial range. Previous gyrokinetic modeling for NT plasmas at TCV and DIII-D also showed a close match between experimental and simulated transport fluxes at the modeled radial locations [11, 13, 14]. In TCV, TEM-driven turbulence was found to be dominant and its reduction in NT was key to reduced transport levels. At DIII-D, the relative importance of TEM and ITG modes was shown to depend sensitively on impurity content, particularly Z_{eff}. The AUG case studied in this work introduces a new aspect: proximity to an instability boundary in the edge, beyond which electromagnetic effects, including possible MTM activity, become significant. Whether this behavior arises due to the relatively modest shaping in this discharge remains an open question. Recent linear studies examining the role of aspect ratio and triangularity suggest that MTMs may indeed be important in NT regimes, but that their impact is more pronounced at low aspect ratio [31].

The gyrokinetic simulations performed on these flux matched profiles provide a basis for additional validation studies, and an investigation of the turbulence nature at these radii. A synthetic CECE diagnostic was applied to the flux-matched simulations to compare T_e fluctuation spectra, amplitude, and correlation length between experiment and simulation. These turbulence properties are more fundamental than the fluxes more typically compared between simulation and experiment, and thus provide a more stringent test of the gyrokinetic model. Comparisons of these T_e fluctuation properties were made at the outer three radial locations ($r/a = 0.75$, 0.83, 0.90), where experimental measurements were available. Excellent agreement was found in the spectral shapes between simulated and experimentally measured turbulence, and the fluctuation amplitudes agreed well at $r/a = 0.75$ and 0.83. At $r/a = 0.90$, the $\sim$20% disagreement in fluctuation amplitude between experiment and simulation can be explained by the limitation of the simulated geometry to midplane fluctuations only. The Gaussian fits to correlation coefficients for determining correlation length also agreed between simulation and experiment at $r/a = 0.75$, although the simulated correlation length was larger than the experimental correlation length at $r/a = 0.83$. The validation of these T_e fluctuation quantities, along with the comparison of heat and particle fluxes and kinetic profiles, indicate that ion-scale gyrokinetics successfully captures the turbulent transport for this plasma. The agreement between simulated profiles and turbulent fluctuations and experimental measurements indicates that current models can be used to predict the core conditions of NT plasmas. There are no showstoppers in terms of core plasma physics when using models widely applied to positive triangularity (PT) plasmas to NT plasmas.

The plasma simulated in this paper was the subject of a previous study [9], in which the plasma was modeled using the quasilinear code TGLF-SAT2 [32] and the kinetic profiles were predicted through the ASTRA-TGLF framework. These previous TGLF profile predictions are shown with the new CGYRO profile predictions in figure 18. For the TGLF predictions, an additional electron diffusivity was added inside $\rho_{\text{tor}} = 0.25$ to constrain core T_e profiles to match with experiment. Within the region simulated by CGYRO, the TGLF and CGYRO predictions have excellent agreement and match well with experimental data. This agreement points to the sufficiency of the gyrofluid model for capturing the turbulent transport fluxes and predicting the kinetic profiles in this plasma scenario. However, advantages still remain in using CGYRO to study the detailed nature of turbulence in this plasma, including (1) the ability to capture up-down asymmetry in the equilibrium with the higher order moments included in the Miller geometry, and (2) the ability to capture MTMs, which cannot accurately be represented with TGLF.

Simulations using the flux-matched profiles allow study of the nature of turbulence across the radius for this plasma. Scans of input parameters were performed linearly to understand dominant mode dynamics, and nonlinearly at selected

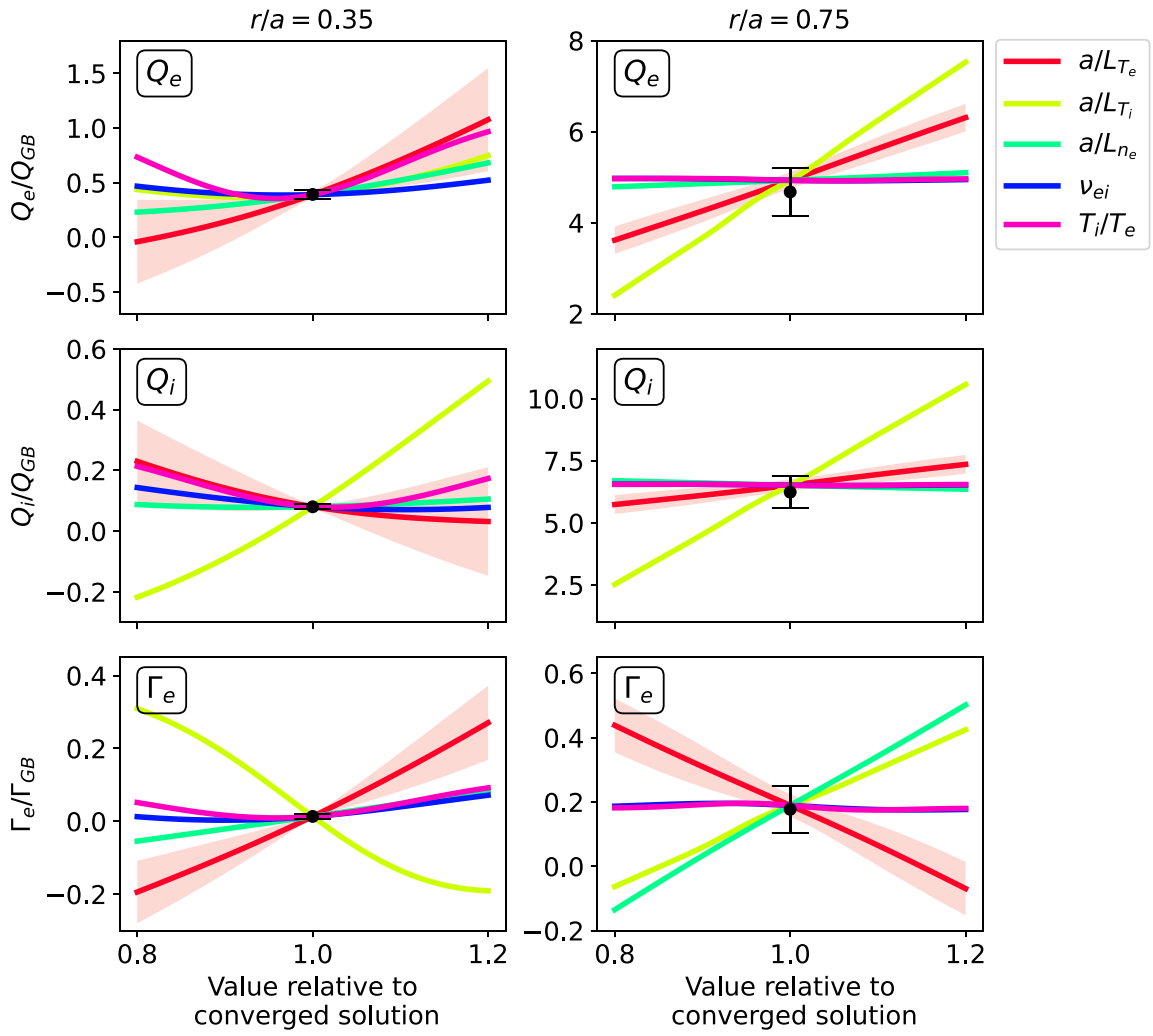

Figure 17. Surrogate model enabled scans at $r/a = 0.35$ and 0.75. Q_e, Q_i, and Γ_e normalized to gyroBohm units predicted from the surrogate model are shown as input parameters (a/L_{T_e}, a/L_{T_i}, a/L_n, ν_{ei}, and T_i/T_e) are individually scanned. The converged CGYRO result is indicated in black. 2σ uncertainties are shown only on a/L_{T_e} for better visualization.

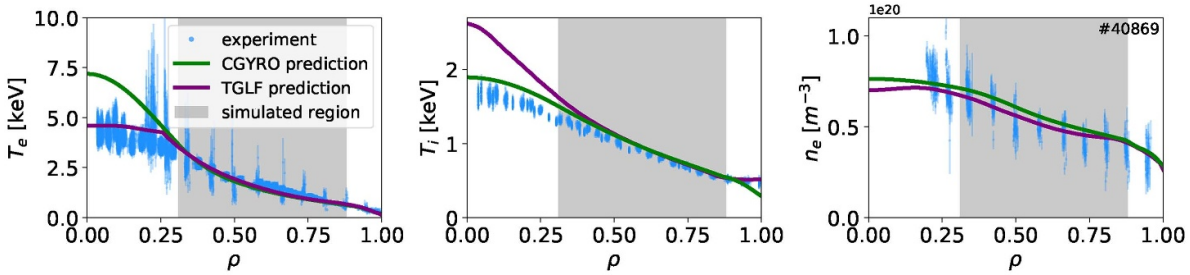

Figure 18. A comparison of profiles predicted with PORTALS-CYGRO (green) and a previous ASTRA-TGLF prediction [9] (purple). Experimental profile measurements are in blue. The region simulated with CGYRO is shaded in gray to indicate the radial region of comparison. The radial coordinate ρ is the square root of the normalized toroidal flux.

locations and for selected parameters. T_e gradient driven TEM was found to be important at the innermost radius, as commonly found with strongly ECRH heated plasmas [33, 34]. ITG was the dominant instability and the dominant driver of both electron and ion heat flux throughout $r/a = 0.55 - 0.83$. At $r/a = 0.90$, the flux-matched simulation appears to sit at an instability boundary. At this location, the turbulence is highly sensitive to a/L_{T_e} both linearly and nonlinearly. When a/L_{T_e} is increased even slightly beyond the converged point, an electromagnetic instability which strongly affects Q_e is found, likely a

MTM. Evidence of this instability is not found experimentally, so the flux-matched case is expected to be below significant growth of this particular mode. It is possible that this instability boundary plays a role in setting the profiles at this location, which is roughly the pedestal top. By sitting immediately at the instability boundary, the T_e profile is extremely stiff and a/L_{T_e} is fixed to the value found in the converged profile. Determining whether the presence of this instability boundary is typical in NT H-mode plasmas will require further study. Understanding the effect of shaping on the nature of turbulence present at different radii will require additional simulations and experiments and is the subject of future work.

NT is an attractive operational scenario for future reactors and further work is needed to fully validate profile prediction frameworks and apply them to predict the performance of future machines [35, 36]. This paper has presented the validation and profile prediction of a particular NT plasma at AUG. The comparison of a matched PT case, following the same flux-matching workflow, would allow for a comparison of turbulence across the radius and an understanding of the difference, if any, in turbulence nature between NT and PT. Even without an experimental comparison, this exercise could be performed computationally to study the effect of shaping on predicted turbulence. A profile prediction with surrogate generation would also be useful to perform for an NT plasma that does not transition to H-mode, such as those with an NT edge common at DIII-D with strong shaping, which were also the subject of recent gyrokinetic modeling work [14]. Overall, this work demonstrates the potential for high fidelity predictive modeling of future NT operational scenarios, contingent on improved understanding of the edge boundary condition.

Acknowledgments

This work has been carried out within the framework of the EUROfusion Consortium, funded by the European Union via the Euratom Research and Training Programme (Grant Agreement No. 101052200 — EUROfusion). Views and opinions expressed are however those of the author(s) only and do not necessarily reflect those of the European Union or the European Commission. Neither the European Union nor the European Commission can be held responsible for them. This work was also supported by the US Department of Energy under Grants DE-SC0014264, DE-SC0006419, DE-SC0017381, and DE-SC0024399. This research was also supported by the U.S. Department of Energy Fusion Energy Sciences Postdoctoral Research Program administered by the Oak Ridge Institute for Science and Education (ORISE) for the DOE. ORISE is managed by Oak Ridge Associated Universities (ORAU) under DOE Contract Number DE-SC0014664. All opinions expressed in this paper are the author's and do not necessarily reflect the policies and views of DOE, ORAU, or ORISE. This research used resources of the National Energy Research Scientific Computing Center (NERSC), a U.S. Department of Energy Office of Science User Facility located at Lawrence Berkeley National Laboratory, operated under Contract No. DE-AC02-05CH11231 using NERSC award FES-ERCAPm224. Some of the simulations performed in this paper were performed on the MIT PSFC Engaging cluster.

Appendix. Simulation inputs

CGYRO inputs parameters for the five simulated radii are given in table A1.

Table A1. Inputs for the CGYRO simulations at the five r/a values.

r/a	0.350	0.550	0.750	0.830	0.900
n_e [$\times 10^{19}$ m^{-3}]	7.099	6.089	4.961	4.604	4.276
T_e [keV]	3.613	1.829	1.042	0.827	0.653
a/L_n	0.413	1.122	0.928	0.937	1.174
a/L_{Te}	3.933	2.875	2.755	3.021	3.730
a/L_{Ti}	1.339	1.569	1.889	2.303	3.072
a/L_{Timp}	1.339	1.569	1.889	2.303	3.072
T_i/T_e	0.415	0.612	0.761	0.810	0.850
n_D/n_e	0.861	0.861	0.861	0.861	0.861
n_{imp}/n_e	2.45×10^{-2}	2.45×10^{-2}	2.45×10^{-2}	2.45×10^{-2}	2.45×10^{-2}
$Z_{\rm eff}$	1.648	1.648	1.648	1.648	1.648
ν_{ee} [c_s/a]	2.34×10^{-2}	7.54×10^{-2}	1.84×10^{-1}	2.67×10^{-1}	3.93×10^{-1}
$\Delta = \frac{\partial R_0}{\partial r}$	−0.067	−0.132	−0.201	−0.228	−0.252
q	−0.997	−1.403	−2.337	−2.885	−3.526
$\hat{s} = \frac{r}{q}\frac{\partial q}{\partial r}$	0.264	1.320	1.944	2.237	2.811
κ	1.254	1.278	1.353	1.400	1.456
$s_\kappa = \frac{r}{\kappa}\frac{\partial \kappa}{\partial r}$	0.014	0.099	0.289	0.404	0.587
δ	−0.017	−0.029	−0.050	−0.064	−0.080
$s_\delta = \frac{r}{\delta}\frac{\partial \delta}{\partial r}$	−0.019	−0.029	−0.113	−0.162	−0.230
ζ	3.30×10^{-4}	-1.07×10^{-3}	-8.91×10^{-3}	-1.58×10^{-2}	-2.63×10^{-2}
$s_\zeta = \frac{r}{\zeta}\frac{\partial \zeta}{\partial r}$	5.00×10^{-4}	-7.72×10^{-3}	-4.98×10^{-2}	-9.18×10^{-2}	-1.88×10^{-1}
$\gamma_{E\times B}(a/c_s)$	-1.37×10^{-2}	-3.11×10^{-2}	-7.27×10^{-3}	-5.28×10^{-3}	-8.64×10^{-3}
$\gamma_p(a/c_s)$	1.37×10^{-1}	2.77×10^{-1}	7.82×10^{-2}	6.31×10^{-2}	1.16×10^{-1}
M	9.54×10^{-2}	7.61×10^{-2}	5.85×10^{-2}	6.26×10^{-2}	5.80×10^{-2}
β_e	1.05×10^{-2}	3.98×10^{-3}	1.39×10^{-3}	8.85×10^{-4}	2.76×10^{-4}
$B_{\rm unit}$ [T]	−3.138	−3.358	−3.872	−4.161	−4.512
B [T]	2.259	2.149	2.065	2.038	2.018

ORCID iDs

R. Bielajew 0000-0002-9578-368X
B. Vanovac 0000-0003-4031-9318
N.T. Howard 0000-0002-8787-6309
P. Rodriguez-Fernandez 0000-0002-7361-1131
G.D. Conway 0000-0002-3947-4268
T. Happel 0000-0003-4364-9363
C. Holland 0000-0001-6029-2306
P. Mantica 0000-0001-5939-5244
J. Schellpfeffer 0000-0002-8687-4475

References

[1] Naulin V. 2007 Turbulent transport and the plasma edge *Plasma-Surf. Interact.-17* **363–365** 24–31
[2] Rodriguez-Fernandez P., Howard N.T., Saltzman A., Kantamneni S., Candy J., Holland C., Balandat M., Ament S. and White A.E. 2024 Enhancing predictive capabilities in fusion burning plasmas through surrogate-based optimization in core transport solvers *Nucl. Fusion* **64** 076034
[3] Rodriguez-Fernandez P., Howard N.T. and Candy J. 2022 Nonlinear gyrokinetic predictions of SPARC burning plasma profiles enabled by surrogate modeling *Nucl. Fusion* **62** 076036
[4] Rodriguez-Fernandez P., Howard N.T., Saltzman A., Shoji L., Body T., Battaglia D.J., Hughes J.W., Candy J., Staebler G.M. and Creely A.J. 2024 Core performance predictions in projected SPARC first-campaign plasmas with nonlinear CGYRO *Phys. Plasmas* **31** 062501
[5] Howard N.T., Rodriguez-Fernandez P., Holland C. and Candy J. 2024 Prediction of performance and turbulence in ITER burning plasmas via nonlinear gyrokinetic profile prediction *Nucl. Fusion* **65** 016002
[6] White A.E. 2019 Validation of nonlinear gyrokinetic transport models using turbulence measurements *J. Plasma Phys.* **85** 925850102
[7] Happel T., Pütterich T., Told D., Dunne M., Fischer R., Hobirk J., McDermott R.M. and Plank U. (the ASDEX Upgrade Team) 2022 Overview of initial negative triangularity plasma studies on the ASDEX Upgrade tokamak *Nucl. Fusion* **63** 016002
[8] Vanovac B. *et al* (the ASDEX Upgrade Team and the EUROfusion WPTE Team) 2024 Pedestal properties of negative triangularity discharges in ASDEX Upgrade *Plasma Phys. Control. Fusion* **66** 115005
[9] Aucone L. *et al* (the EUROfusion WPTE Team and the ASDEX Upgrade Team) 2024 Experiments and modelling of negative triangularity ASDEX Upgrade plasmas in view of DTT scenarios *Plasma Phys. Control. Fusion* **66** 075013
[10] Marinoni A., Brunner S., Camenen Y., Coda S., Graves J.P., Lapillonne X., Pochelon A., Sauter O. and Villard L. 2009 The effect of plasma triangularity on turbulent transport: modeling TCV experiments by linear and non-linear gyrokinetic simulations *Plasma Phys. Control. Fusion* **51** 055016
[11] Merlo G., Fontana M., Coda S., Hatch D., Janhunen S., Porte L. and Jenko F. 2019 Turbulent transport in TCV plasmas with positive and negative triangularity *Phys. Plasmas* **26** 102302
[12] Mariani A. *et al* (the EUROfusion Tokamak Exploitation Team, the TCV Team and the ASDEX Upgrade Team) 2024

Negative triangularity scenarios: from TCV and AUG experiments to DTT predictions *Nucl. Fusion* **64** 106024
[13] Balestri A. *et al* (the TCV Team and the EUROfusion Tokamak Exploitation Team) 2024 Experiments and gyrokinetic simulations of TCV plasmas with negative triangularity in view of DTT operations *Plasma Phys. Control. Fusion* **66** 065031
[14] Marinoni A., Austin M.E., Candy J., Chrystal C., Haskey S.R., Porkolab M., Rost J.C. and Scotti F. 2024 Nonlinear gyrokinetic modelling of high confinement negative triangularity plasmas *Nucl. Fusion* **64** 086045
[15] Candy J., Belli E.A. and Bravenec R.V. 2016 A high-accuracy Eulerian gyrokinetic solver for collisional plasmas *J. Comput. Phys.* **324** 73–93
[16] Pankin A.Y., Breslau J., Gorelenkova M., Andre R., Grierson B., Sachdev J., Goliyad M. and Perumpilly G. TRANSP integrated modeling code for interpretive and predictive analysis of tokamak plasmas (arXiv:2406.07781) [physics.plasm-ph]
[17] Kurzan B. and Murmann H.D. 2011 Edge and core Thomson scattering systems and their calibration on the ASDEX Upgrade tokamak *Rev. Sci. Instrum.* **82** 103501
[18] Rathgeber S.K., Barrera L., Eich T., Fischer R., Nold B., Suttrop W., Willensdorfer M. and Wolfrum E. (the ASDEX Upgrade Team) 2012 Estimation of edge electron temperature profiles via forward modelling of the electron cyclotron radiation transport at ASDEX Upgrade *Plasma Phys. Control. Fusion* **55** 025004
[19] Viezzer E., Pütterich T., Dux R. and McDermott R.M. (ASDEX Upgrade Team) 2012 High-resolution charge exchange measurements at ASDEX Upgrade *Rev. Sci. Instrum.* **83** 103501
[20] McDermott R.M. *et al* 2017 Extensions to the charge exchange recombination spectroscopy diagnostic suite at ASDEX Upgrade *Rev. Sci. Instrum.* **88** 073508
[21] Freethy S.J., Conway G.D., Classen I., Creely A.J., Happel T., Köhn A., Vanovac B. and White A.E. 2016 Measurement of turbulent electron temperature fluctuations on the ASDEX Upgrade tokamak using correlated electron cyclotron emission *Rev. Sci. Instrum.* **87** 11E102
[22] Creely A.J., Freethy S.J., Burke W.M., Conway G.D., Leccacorvi R., Parkin W.C., Terry D.R. and White A.E. 2018 Correlation electron cyclotron emission diagnostic and improved calculation of turbulent temperature fluctuation levels on ASDEX Upgrade *Rev. Sci. Instrum.* **89** 053503
[23] Rempel T.D., Gandy R.F. and Wootton A.J. 1994 Density fluctuation effects on electron cyclotron emission correlation measurements in optically gray plasmas *Rev. Sci. Instrum.* **65** 2044–8
[24] Arbon R., Candy J. and Belli E.A. 2020 Rapidly-convergent flux-surface shape parameterization *Plasma Phys. Control. Fusion* **63** 012001
[25] Belli E.A. and Candy J. 2008 Kinetic calculation of neoclassical transport including self-consistent electron and impurity dynamics *Plasma Phys. Control. Fusion* **50** 095010
[26] Terry P.W., Greenwald M., Leboeuf J.-N., McKee G.R., Mikkelsen D.R., Nevins W.M., Newman D.E. and Stotler D.P. (Task Group on Verification and Validation, U.S. Burning Plasma Organization and U.S. Transport Task Force) 2008 Validation in fusion research: towards guidelines and best practices *Phys. Plasmas* **15** 062503
[27] Holland C., White A.E., McKee G.R., Shafer M.W., Candy J., Waltz R.E., Schmitz L. and Tynan G.R. 2009 Implementation and application of two synthetic diagnostics for validating simulations of core tokamak turbulence *Phys. Plasmas* **16** 052301
[28] Cabrera P.A.M. *et al* 2023 Isotope effects on energy transport in the core of ASDEX-Upgrade tokamak plasmas: turbulence measurements and model validation *Phys. Plasmas* **30** 082304
[29] Howard N.T., Holland C., White A.E., Greenwald M., Candy J. and Creely A.J. 2016 Multi-scale gyrokinetic simulations: comparison with experiment and implications for predicting turbulence and transport *Phys. Plasmas* **23** 056109
[30] Creely A.J., Rodriguez-Fernandez P., Conway G.D., Freethy S.J., Howard N.T. and White A.E. (the ASDEX Upgrade Team) 2019 Criteria for the importance of multi-scale interactions in turbulent transport simulations *Plasma Phys. Control. Fusion* **61** 085022
[31] Balestri A., Ball J., Coda S., Cruz-Zabala D.J., Garcia-Munoz M. and Viezzer E. 2024 Physical insights from the aspect ratio dependence of turbulence in negative triangularity plasmas *Plasma Phys. Control. Fusion* **66** 075012
[32] Staebler G.M., Belli E.A., Candy J., Kinsey J.E., Dudding H. and Patel B. 2021 Verification of a quasi-linear model for gyrokinetic turbulent transport *Nucl. Fusion* **61** 116007
[33] White A.E. *et al* 2010 Measurements of the cross-phase angle between density and electron temperature fluctuations and comparison with gyrokinetic simulations *Phys. Plasmas* **17** 056103
[34] Wang L., Peng S. and Diamond P.H. 2016 Intrinsic rotation drive by collisionless trapped electron mode turbulence *Phys. Plasmas* **23** 042309
[35] Rutherford G *et al* (The MANTA Collaboration) 2024 MANTA: a negative-triangularity NASEM-compliant fusion pilot plant *Plasma Phys. Control. Fusion* **66** 105006
[36] Paz-Soldan C. *et al* 2024 Simultaneous access to high normalized density, current, pressure and confinement in strongly-shaped diverted negative triangularity plasmas *Nucl. Fusion* **64** 094002